Earth and Planetary Science Letters 596 (2022) 117795

Contents lists available at ScienceDirect

Earth and Planetary Science Letters

www.elsevier.com/locate/epsl

Coevolution of sedimentary and strongly peraluminous granite phosphorus records

Claire E. Bucholz

Division of Geological and Planetary Sciences, California Institute of Technology, Pasadena, CA 91125, United States of America

ARTICLE INFO

Article history:
Received 21 April 2022
Received in revised form 13 July 2022
Accepted 26 August 2022
Available online 9 September 2022
Editor: A. Webb

Keywords:
phosphorus
peraluminous
S-type
granite

ABSTRACT

Phosphorus plays an important role in both surface biological cycles as a critical macronutrient and in magmatic systems as the backbone for trace element-rich phosphate minerals. Phosphorus cycling between igneous and sedimentary systems throughout Earth history has had potentially profound effects on biogeochemical cycles. Previous studies have focused on the impacts of enhanced contribution of phosphorus from igneous rocks on marine phosphorus budgets. In contrast, the effect of changing sedimentary phosphorus abundances on the phosphorus budget of magmas has not been investigated. Here I present a compilation of phosphorus concentrations in strongly peraluminous granites (SPGs), which are derived through the partial melting of sedimentary rocks, spanning the past ~3.5 billion years. Maximum phosphorus concentrations of SPGs increase abruptly in the Phanerozoic, closely following a similar, previously documented increase in phosphorus concentrations in marine siliciclastic sediments deposited after 720 Ma. The effect of metamorphic, magmatic, and subsolidus processes on SPG bulk-rock phosphorus concentrations are considered in turn. Lower average bulk-rock phosphorus concentrations in SPGs derived from metasedimentary rocks deposited prior to 720 Ma likely reflect lower phosphorus concentrations of their metasedimentary sources. The SPG compilation both confirms previous observations of phosphorus abundances in the marine sedimentary record and provides an alternative archive in that it integrates large volumes of continental shelf to slope sedimentary rocks. A clear shift in the crustal phosphorus cycle is documented with the initiation of enhanced recycling of sedimentary phosphorus into the igneous crust, where it can be again weathered and returned to the ocean to fuel further photosynthesis. Although phosphorus concentrations in zircon have been used to distinguish between derivation from strongly peraluminous "S-type" from metaluminous "I-type" granites, the results presented here suggest that phosphorus concentrations in SPGs have a time dependency and that phosphorus concentrations in zircon from SPGs may vary similarly in time.

1. Introduction

Phosphorus is an important element in biogeochemical and sedimentary surface environments as well as igneous systems. As an important macronutrient, phosphorus limits primary productivity in the oceans on geologic timescales (Tyrrell, 1999). Consequently there has been intense interest in constraining the past marine phosphorus cycle (Bjerrum and Canfield, 2002; Reinhard et al., 2017). In igneous rocks, phosphate minerals are important hosts for trace elements and volatiles (cf., Piccoli and Candela, 2002). Previous studies have demonstrated potential links between phosphorus concentrations in igneous rocks and marine phosphorus budgets. For example, secular increases in phosphorus concentrations in igneous rocks due to decreases in the degree of mantle melting (Cox et al., 2018) and emplacement of phosphorus-rich large igneous provinces in the Neoproterozoic (Horton, 2015) have been proposed to have increased the phosphorus flux to oceans, enhanced primary productivity and oxygen photosynthesis, and contributed to increases in atmospheric oxygen.

Here I explore the reverse scenario where variations in the marine phosphorus cycle could have influenced phosphorus abundances in igneous rocks. Although estimates of marine phosphate levels are difficult to obtain from the sedimentary record and not agreed on (Bjerrum and Canfield, 2002; Kipp and Stüeken, 2017; Planavsky et al., 2010; Rasmussen et al., 2021), secular variations in phosphorus concentrations in the sedimentary record exist. For example, phosphorites are absent from the Archean rock record, uncommon in the Proterozoic, and only become abundant in the Neoproterozoic onward (Cook and McElhinny, 1979; Holland, 2005). Further, secular variations in P/Fe ratios in iron formations and iron-oxide-rich hydrothermal sediments have been

E-mail address: cbucholz@caltech.edu.

https://doi.org/10.1016/j.epsl.2022.117795
0012-821X/

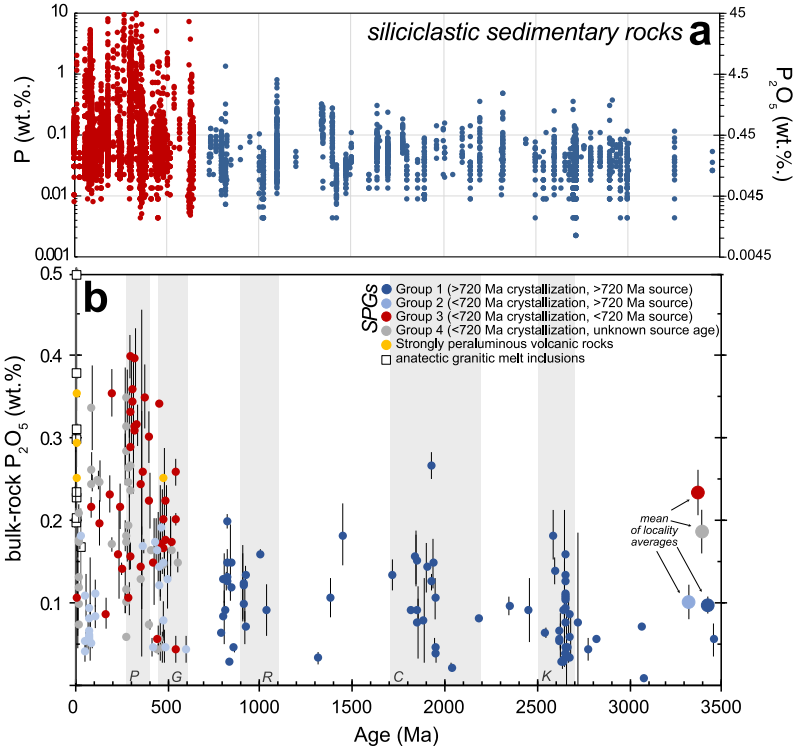

Fig. 1. Phosphorus contents in sedimentary and igneous records from 0 to 3500 million years ago. (a) Phosphorus (P) concentrations (log scale) of fine-grained, marine siliciclastic sedimentary rocks from Reinhard et al. (2017). Pre- and post-720 Ma rocks are shown in blue and red, respectively. (b) Average P_2O_5 concentrations for SPG and peraluminous volcanic localities plotted against their crystallization ages. Error bars are 2 s.e.m. (see Table S2). Averages of Group 1, 2, 3, and 4 locality averages are shown on left side of the figure as large coloured circles. Here, and in all figures, P_2O_5 concentrations plotted are normalized to an anhydrous bulk-rock major element oxide total. Average values of P_2O_5 concentrations in granitic melt inclusions from in various minerals (garnet, cordierite, andalusite, ilmenite) from anatectic terranes or metapelitic enclaves in volcanic rocks are shown as open squares for reference. Melt inclusion data is from metapelitic enclaves in the El Hoyazo dacite and Mazarrón (Spain), metatexites from Ronda (Spain), and the Gruf Complex (Italy) (Acosta-Vigil et al., 2007, 2010; Bartoli et al., 2013; Cesare et al., 2015; Gianola et al., 2021). Grey vertical bars show times of supercontinent assemblies with capital letters indicating the supercontinents; K: Kenorland, C: Columbia, R: Rodinia, G: Gondwana, and P: Pangea. (For interpretation of the colours in the figure(s), the reader is referred to the web version of this article.)

interpreted as changes in the marine phosphate reservoir (Bjerrum and Canfield, 2002; Planavsky et al., 2010). Of particular interest to this study, phosphorus abundances in ancient marginal marine sediments (*i.e.*, fine-grained siliciclastic sedimentary rocks) dramatically increase in maximum values (from ~0.1 to 10 wt.%) and variability at 700 to 800 million years ago (Reinhard et al., 2017) (Fig. 1a). Although the exact cause of low phosphorus abundances in Archean and Proterozoic sedimentary rocks are debated, most agree it is related to low levels of dissolved O_2 in the oceans and limited burial of authigenic apatite (Kipp and Stüeken, 2017; Planavsky et al., 2010; Reinhard et al., 2017). For example, prior to the late Neoproterozoic, ferruginous (anoxic and Fe-rich) oceans could have led to efficient scavenging and removal of bioavailable phosphorus from the ocean surface through formation of a variety of Fe-P-bearing phases (Halevy et al., 2017; Zegeye et al., 2012) or co-precipitation of phosphorus on iron oxides (Bjerrum and Canfield, 2002). Alternatively, the overall size of the marine phosphorus reservoir (and thus phosphorus concentrations recorded in sedimentary rocks) could have been limited by the minimal liberation of phosphorus during the remineralization of organic carbon in anoxic Archean and Proterozoic oceans (Kipp and Stüeken, 2017).

I explore whether this shift in siliciclastic sedimentary phosphorus abundances influenced the igneous rock record through an examination of a specific rock type, strongly peraluminous granites (SPGs), which have bulk-rock aluminum saturation indices [ASI = molar Al/(Ca+Na+K)] > 1.1. SPGs are also commonly referred to as "S-type" granites because they are inferred to have formed from melting of (meta-)sedimentary rocks. [Note: Here, I choose to call them SPGs as this traditional "alphabet" classification has been replaced by a purely geochemical classification which eliminates ambiguity associated with previous granite classifications (Frost et al., 2001)]. SPGs represent a fundamental limb in the rock cycle where sedimentary rocks are recycled into the igneous rock record and can record information about their sedimentary source rock compositions (Bucholz and Spencer, 2019; Chappell and White, 1992; Sylvester, 1998). I test whether temporal changes in sedimentary rock phosphorus concentrations, which are thought to be intimately linked to changes in marine redox conditions and biogeochemical cycling, are also translated to the SPG record through (1) compiling SPG bulk-rock analyses from published literature and providing new analyses of SPGs to complement the compilation and (2) critically analyzing what phosphorus concentrations in SPGs represent.

2. Methods

2.1. X-ray fluorescence

22 samples of Archean and Proterozoic SPGs were analyzed for major and trace element concentrations via X-ray fluorescence at Caltech following methods described in Bucholz and Spencer (2019). Sample information is given in the Supplementary Material and new data is provided in Table S1.

2.2. Strongly peraluminous granite compilation

Strongly peraluminous granite bulk-rock major and trace element analyses were compiled from published literature from localities where researchers previously concluded that they formed

through the partial melting of siliciclastic sedimentary rocks, such as metapelites and metagraywackes. A small number (n = 49) of analyses for strongly peraluminous rhyolitic to dacitic volcanic rocks also thought to be formed via partial melting of sedimentary rocks (e.g., from the Macusani volcanic field, Pichavant et al., 1988) were also included in the compilation.

In addition to the presence of peraluminous indicator minerals (e.g., muscovite, garnet, tourmaline, etc.) and bulk-rock major element chemistry indicating derivation from an aluminous sedimentary source, SPGs in the compilation have been linked to metasedimentary sources through a combination of field relationships, radiogenic and stable isotopic data, and examination of magmatic and inherited zircon populations. For example, in some localities field associations of SPG plutons with prograde metasedimentary metamorphic sequences from low grade to partial anatexis are documented and provide a direct link from sedimentary source to granitic melt (e.g., Breaks and Moore, 1992; Solar and Brown, 2001). In addition, unradiogenic Nd and Hf isotopes, radiogenic Sr isotopes, and elevated oxygen isotopes in both whole rocks and mineral separates are used as evidence of derivation from a sedimentary source for SPGs compiled here. In particular, the combined use of zircon Hf and O isotopes has proven to be particularly effective at identifying granites derived from melting of metasedimentary rocks (e.g., Hopkinson et al., 2017). Although disequilibrium of the Sr, Nd, and Hf isotopes during crustal anatexis can and certainly does occur (e.g., Ayres and Harris, 1997; Zeng et al., 2005; Zhang et al., 2020), melts of metasedimentary rocks should still have relatively radiogenic Sr and unradiogenic Nd and Hf isotopes relative to mantle values. Further, detailed characterization of U-Pb ages and O isotopes of zircon populations in some SPGs has revealed an abundance of inherited cores from metasedimentary protoliths.

Only analyses with 68 to 80 wt.% SiO_2 and major element oxide totals between 98 to 102 wt.% were included in the compilation. The first restriction was imposed to ensure broadly silicic compositions as apatite solubility in melts is strongly influenced by melt SiO_2 (Harrison and Watson, 1984) and low SiO_2 concentrations in SPGs can potentially indicate incorporation of significant, inherited restitic or peritectic material from their source regions (Stevens et al., 2007; White and Chappell, 1977). The second restriction was imposed to remove any poor-quality bulk-rock analyses. Last, any samples described explicitly as pegmatitic were excluded as it is difficult to meaningfully capture the "bulk" composition of a pegmatite due to their coarse grain size and they likely represent hydrothermal, rather than magmatic compositions. Further filtering is considered in Section 4.3 to assess the effect of magmatic differentiation on phosphorus concentrations. A total of 2,279 analyses were included in the final dataset. All compiled SPG and volcanic rock data, in addition to the newly obtained analyses (see Section 2.1), are provided in Table S1.

Compiled analyses were then grouped by geographical location and age to obtain a locality average. In most cases, this was straightforward as there was either a single isolated SPG pluton or several geographically proximal SPG plutons with similar crystallization ages. When several plutons in a single geographical location had distinct crystallization ages, samples were grouped by pluton and each pluton was considered a distinct locality. In more complicated cases (e.g., a field or batholith composed of multiple SPG plutons), analyses were grouped by pluton (or a close association of plutons) based on descriptions given in the original references. As an example, the reader is referred to the Paleozoic Cornubian batholith of SW England, comprising six major plutons and numerous smaller granitic stocks. In this situation, granites were grouped into individual localities associated with either the six major plutons (Bodmin, Carnmenellis, Dartmoor, St. Austell, Tregonning, and Land's End) or associated minor stocks instead of consolidating all analyses from the batholith into a single average.

Each locality was then characterized by (1) its crystallization age and (2) the inferred depositional age of its source rock. For these ages I relied on the interpretation of the authors of the original studies of the SPGs. Crystallization ages of SPGs are relatively straightforward to obtain based on various geochronological methods primarily including in-situ zircon or monazite U-Pb ages. When available, estimates of depositional ages of the metasedimentary source rocks were generally constrained based on either field observations linking SPGs to specific metasedimentary units as sources, U-Pb ages of inherited zircon populations, or Nd or Hf isotopic mantle depletion ages. Because Nd and Hf isotopes of SPGs may not reflect that of their source due to isotopic disequilibrium during melting (Zeng et al., 2005; Zhang et al., 2020), the latter criteria was considered less robust than the first two and the source rock depositional ages were considered unknown.

Based on crystallization and source rock ages, localities were then grouped into four categories. First, 720 Ma was used as a primary boundary for a crystallization age following previously observed changes in the phosphorus abundances in sedimentary siliciclastic rocks (Fig. 1a; Reinhard et al., 2017). Group 1 SPGs are those that have both a crystallization age and (by necessity) source rocks older than 720 Ma. SPGs with crystallization ages <720 Ma were then placed into three different groups based on the age of their source rocks. Group 2 SPGs are classified as those with a sedimentary source with a >720 Ma depositional age. Group 3 SPGs are those with depositional ages for sedimentary source rocks <720 Ma. Finally, Group 4 SPGs are those with unknown or loosely constrained depositional ages for their source rocks (e.g., via Nd mantle depletion ages). A total of 693, 242, 965, and 375 analyses were compiled for Groups 1, 2, 3, and 4 respectively. Strongly peraluminous volcanic rocks (n = 49) were not included in the groups but are all from localities with Phanerozoic crystallization ages. Compiled SPG analyses are grouped by locality in Table S1. Locality details (including lithology, geochronology, and inferred source rock depositional ages) and averages are given in Table S2.

3. Results

Locality average P_2O_5 versus crystallization age are shown in Fig. 1b. No SPG localities were identified with crystallization ages between 610-790 Ma, and only three localities were identified between 1100-1700 Ma, consistent with SPGs forming dominantly during the supercontinent assembly and major collisional orogenies (Fig. 1b). The most salient feature of the SPG compilation is an increase in maximum P_2O_5 concentrations and variability in SPGs (and peraluminous volcanic rocks) in Group 3 and 4 SPGs as compared to Group 1 and 2 (Fig. 1b). When all compiled analyses are considered, the lower P_2O_5 values in Groups 1 and 2 and higher values for Group 3 and 4 are readily apparent in histograms and cumulative frequency distributions (Fig. 2).

The mean P_2O_5 of all samples from Group 1, 2, 3, and 4 are 0.105±0.005, 0.123±0.008, 0.241±0.009, 0.215±0.010 (±2 standard error of the mean (s.e.m.)) (Fig. 2a-d). The mean P_2O_5 of Group 1 and Group 2 SPGs compared to Group 3 and Group 4 SPGs are statistically distinguishable ($P<0.001$, Wilcoxon rank-sum test). The mean P_2O_5 of Group 1, 2, 3, and 4 locality averages is 0.095±0.012 wt.% (±2 s.e.m., n = 72), 0.101±0.020 (2 s.e.m., n = 25), 0.230±0.031 wt.% (2 s.e.m., n = 38), and 0.180±.029 (2 s.e.m., n = 35) (Fig. 1b). These values are within error of the mean of all the samples indicating that one locality for which there are many analyses is not dominating the distributions shown in Fig. 2. Group 3 locality averages fall within the range of average P_2O_5 concentrations reported for granitic melt inclusions from anatectic rocks (0.2-0.5 wt.%; Fig. 1b) which record primary melt compositions resulting from the anatexis of Phanerozoic sedimentary rocks

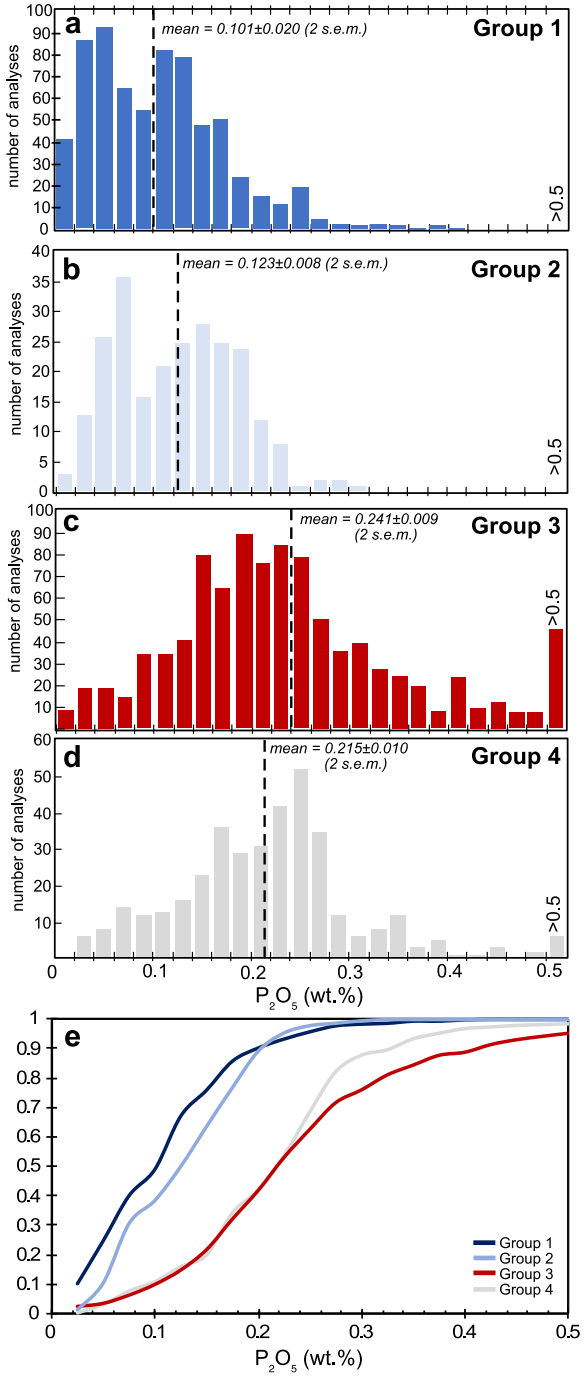

Fig. 2. Histograms and cumulative frequency distributions of SPG by group. Histograms of all analyses included in (a) Group 1, (b) Group 2, (c) Group 3, and (d) Group 4. (e) Cumulative frequency distributions of P_2O_5 concentrations for all analyses from Group 1 through 4 SPGs.

(Acosta-Vigil et al., 2010, 2007; Bartoli et al., 2013; Cesare et al., 2015).

4. Phosphorus concentrations in strongly peraluminous granites: what do they reflect?

The similarity between temporal patterns in phosphorus concentrations in siliciclastic metasedimentary rocks and SPGs is striking (Fig. 1), however phosphorus concentrations in SPGs are not necessarily expected to reflect that of their source sedimentary rocks. Phosphorus may be fractionated during metamorphism and partial melting of metasedimentary rocks, as well as crystallization-differentiation and cooling of granitic magmas (Fig. 3). I discuss each process in turn and how it could influence the interpretation of the temporal variations observed in the SPG literature compilation.

4.1. Phosphorus during prograde metamorphism and partial melting

Apatite and monazite are the dominant hosts for phosphorus and light rare earth elements (LREE) in Al-rich siliciclastic metamorphic rocks (Bea, 1996; Spear and Pyle, 2002). Field studies of prograde metasedimentary sequences have documented that although local redistribution and growth of phosphates occurs during prograde metamorphism, bulk-rock P_2O_5 remain relatively unchanged until partial melting occurs (Bea and Montero, 1999; Wing et al., 2003). Although phosphorus mobility may occur during focused fluid flow event (e.g., as preserved in veins and adjacent lithologies), redistribution of phosphate phases is likely local (Ague, 2017). Thus, prior to partial melting phosphorus concentrations of sedimentary rocks during prograde metamorphism should be broadly conserved (Fig. 3a).

Upon partial melting, apatite and monazite break down to saturate the anatectic melt in phosphorus and LREE (Duc-Tin and Keppler, 2015; Harrison and Watson, 1984; Montel, 1993; Pichavant et al., 1992; Stepanov et al., 2012; Wolf and London, 1994). The salient features of apatite and monazite break down are summarized here, but readers are referred to previous detailed reviews of the factors controlling apatite and monazite dissolution in an anatectic melt (Harrison and Watson, 1984; Yakymchuk, 2017; Yakymchuk and Acosta-Vigil, 2019). Apatite (with 39-42 wt.% P_2O_5) is the main contributor of phosphorus to the melt (London et al., 1999; Yakymchuk, 2017; Yakymchuk and Acosta-Vigil, 2019). Monazite dissolution will also liberate phosphorus into a partial melt, however the contribution of phosphorus from monazite is negligible compared to that liberated from apatite breakdown due to it containing less P_2O_5 (~29 wt.% in monazite) and its lower solubility in peraluminous melts (Montel, 1993), but also due to its lower modal abundances in metasedimentary rocks.

Assuming that most of the phosphorus in the metasedimentary source is hosted in apatite (though see 4.1.1 for caveats), partial melts of metasedimentary rocks will be buffered at the P_2O_5 content of apatite saturation if the source retains apatite that is in continual communication with the melt (Harrison and Watson, 1984; Watson and Capobianco, 1981; Yakymchuk, 2017). The behaviour of apatite and monazite during partial melting of metapelites was explored in significant detail by Yakymchuk (2017) via coupling of thermodynamic phase equilibria modelling with solubility equations for apatite and monazite along isobaric heating paths (Fig. 4). For metapelitic sources with higher bulk P_2O_5 (0.3-0.5 wt.%) apatite is expected to remain stable in the source region up to ultrahigh temperature conditions (>900 °C) and melt P_2O_5 will be buffered at apatite saturation values. In source rocks with 0.1 wt.% P_2O_5 apatite is completely consumed between 800-850 °C. In sources with ≤0.1 wt.% P_2O_5, apatite will be exhausted at even lower temperatures and anatectic melts produced at higher temperatures will not be saturated (Fig. 4). After exhaustion of apatite, the P_2O_5 of anatectic melts decrease with progressive partial melting as apatite saturation is not maintained (Fig. 4). Although differences in pressures and styles (e.g., closed versus open system) melting will result in different temperatures at which apatite is exhausted, the general form of the modelled melt P_2O_5 concentration with temperature remains the same.

The modelling results of Yakymchuk (2017) can be applied to sources with average pre- and post-720 Ma bulk sedimentary P_2O_5 of ~0.1 wt.% and ~0.5 wt.%, respectively (Reinhard et al., 2017). During partial melting, a metapelite with 0.1 wt.% P_2O_5 will be depleted in apatite at ~830-840 °C when melt P_2O_5 concentrations

reach ~0.3 wt.%. With progressive depletion beyond apatite exhaustion P_2O_5 will decrease from 0.3 to 0.15 at 950 °C. In the likely scenario where either not all the bulk-rock phosphorus is hosted in apatite or if apatite does not maintain equilibrium with the melt (see section 4.1.1 and Fig. 3b) the effective bulk-rock P_2O_5 concentration available to participate in the melting process will be lower. Lower effective bulk-rock P_2O_5 partial melting scenarios are shown for 0.05 and 0.01 wt.% P_2O_5 in Fig. 4 (personal communication C. Yakymchuk). Apatite is exhausted at lower temperatures (~800 and ~740 °C, respectively) and anatectic melt P_2O_5 concentrations reach a maximum of 0.12 and 0.25 wt.% at the point of apatite exhaustion and then decrease with increasing temperature, reproducing the range of P_2O_5 concentrations observed in Group 1 and 2 SPGs (<0.2 wt.%). Further, the Wolf and London (1994) apatite solubility model used in these calculations does not include a temperature dependency, which renders the modelled temperature of apatite exhaustion from the source and onset of the decrease in melt P_2O_5 maximum values. In contrast, for an average post-720 Ma sedimentary source with ~0.5 wt.% P_2O_5, melts will remain saturated with respect to apatite and at temperatures appropriate for biotite-dehydration melting (800-850 °C) reach values of 0.3-0.4 wt.% P_2O_5, consistent with Group 3 SPG bulk-rock P_2O_5 concentrations (Fig. 1b, 4). Apatite-saturated melt P_2O_5 concentrations are also consistent with analyses of granitic melt inclusions which are thought to represent primary anatectic melts (e.g., Cesare et al., 2015; Fig. 1b).

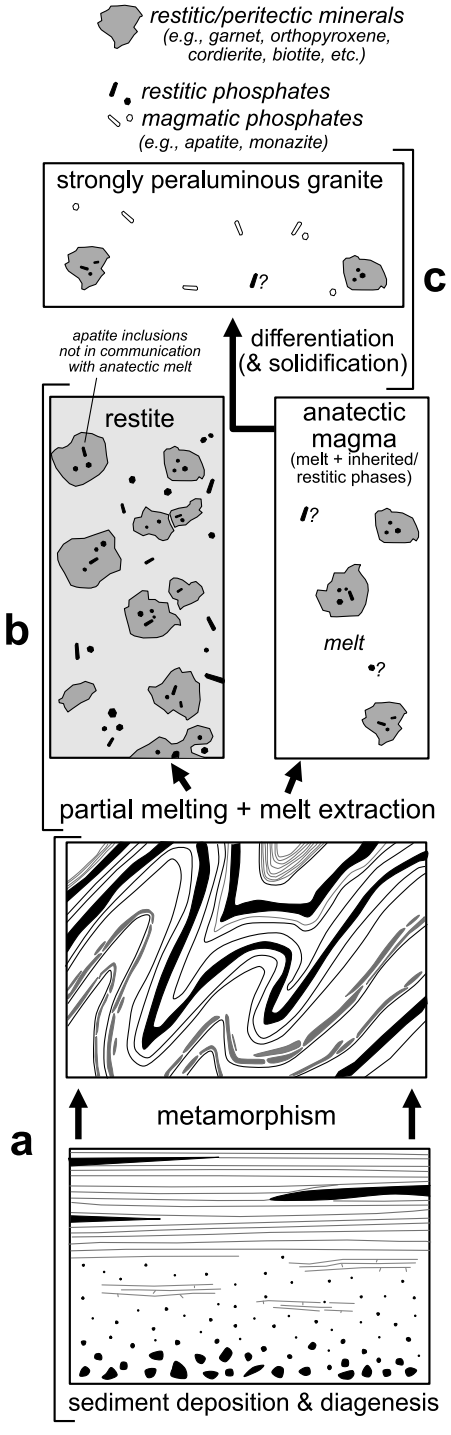

Fig. 3. Processes controlling phosphorus concentrations in SPGs from sedimentary source to crystallization. (a) Sedimentary deposition, diagenesis, and metamorphism are expected to result in local redistribution of phosphorus. (b) During partial melting, phosphates (primarily apatite) in the source rock will break down to saturate the anatectic melt in phosphorus. Whether apatite remains in the restite during partial melting depends on the degree/temperature of melting, original source rock phosphorus contents, and the ability for apatite to maintain equilibrium with the melt. Source rocks with phosphorus concentrations less than that required to achieve apatite saturation will eventually be depleted, with the depletion temperature decreasing with lower source rock phosphorus concentrations. Apatite not in communication with the anatectic melt (e.g., through enclosure in other phases) will not break down and remain in the restite. The anatectic magma will consist of both granitic melt and potentially inherited/restitic phases. Apatite is unlikely to be inherited as an isolated phase (i.e., not as an inclusion) due to the high solubility of apatite in peraluminous magmas, (hence the question marks next to those crystals). (c) During differentiation, phosphorus contents in strongly peraluminous anatectic melts are expected to increase due to the late saturation of apatite in these magmas. K/Rb and ASI values will also increase. During solidification, apatite (and potentially monazite) will eventually saturate (shown as open crystals). The white matrix represents other primary magmatic minerals comprising the final solidified SPG (e.g., feldspar, quartz, biotite, muscovite, etc.). The final measured phosphorus concentrations of a SPG will reflect both the evolution of the anatectic melt (during partial melting and crystallization) and any potential inherited restitic material.

4.1.1. Caveats and complications

There are several simplifications in modelling anatectic melt P_2O_5 concentrations assumed in the study of Yakymchuk (2017) (which are discussed in detail within that paper) that may deviate from natural scenarios. First, although apatite and monazite are the main reservoirs of phosphorus in metapelitic rocks, major phases such as garnet, plagioclase, and alkali-feldspar can host significant amounts of phosphorus (e.g., 100 s to 1000 s ppm in garnet; Kohn and Malloy, 2004; Pyle and Spear, 1999). If garnet was an important host of phosphorus, then the amount of P_2O_5 in the rock available for apatite would be lower and P_2O_5 participating in apatite-dissolution reaction to maintain apatite saturation during anatexis would also be lower (Yakymchuk, 2017). With increasing temperature, modal abundances of garnet are expected to increase due to dehydration melting of biotite, resulting in a greater proportion of the bulk phosphorus partitioning into the garnet and more rapid exhaustion of apatite. The behaviour of feldspars is more complicated. During muscovite and biotite-dehydration melting K-feldspar is produced and plagioclase is consumed, the latter of which is enhanced at high pressures (Bartoli, 2021). Thus, the specific effects of phosphorus-bearing silicate growth or consumption during suprasolidus prograde metamorphism on anatectic phosphorus melt compositions will vary with bulk composition and pressure-temperature path. However, in general, the formation of garnet and K-feldspar during suprasolidus prograde metamorphism will decrease the amount of phosphorus available for apatite formation, which would result in apatite exhaustion at even lower temperatures than that predicted in the model results shown in Fig. 4.

Second, the modelling of Yakymchuk (2017) assumes equilibrium between phosphates and anatectic melt. Critically kinetic and textural controls on apatite-melt equilibrium may make this

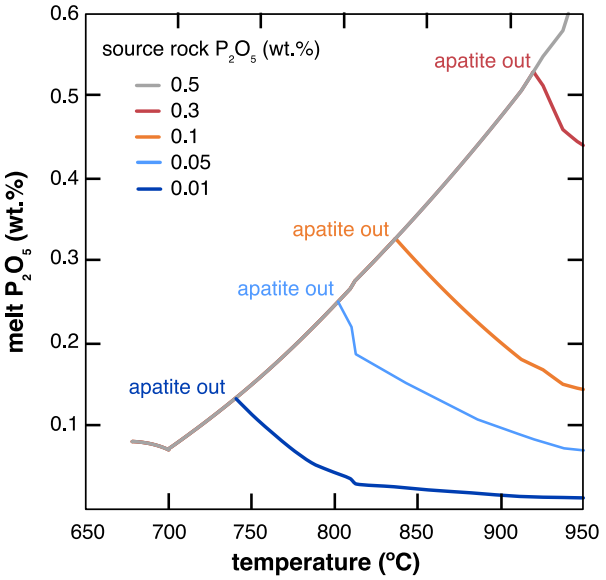

Fig. 4. Modelled anatectic melt P_2O_5 concentrations during partial melting of a metapelite. Closed system model results from Yakymchuk (2017) using thermodynamic phase equilibria coupled with solubility models for apatite and monazite along an isobaric heating path (0.6 GPa). The apatite solubility equation of Wolf and London (1994) is used. Different coloured curves represent different initial source rock bulk P_2O_5 concentrations. Scenarios of 0.05 and 0.01 wt.% were obtained from personal communication with C. Yakymchuk following the modelling approach of Yakymchuk (2017).

assumption invalid. For example, dissolution kinetics can inhibit phosphate break down during anatexis, resulting in undersaturation of the melt in phosphorus and LREE (Ayres and Harris, 1997; Bea, 1996; Zeng et al., 2005). Similarly, apatite and monazite may be included in other major mineral phases such as biotite or garnet (e.g., Nabelek and Glascock, 1995; Watson et al., 1989). Armoring of apatite will inhibit its communication with the melt, resulting in a decreased percentage of P_2O_5 in the bulk (meta-)sedimentary rock available to participate in the partial melting reaction (Fig. 3b). The combined effect of these disequilibrium processes would be to reduce the "effective" bulk-rock and anatectic melt P_2O_5 concentrations below that predicted in equilibrium melting models (see 4.1 and Fig. 4). If it is assumed, for the moment, that the compiled SPGs bulk-rock data represent melt compositions, one interpretation of the temporal trends in Figs. 1 and 2 would be that kinetic and textural inhibition of apatite dissolution in the melt was preferentially occurring in SPGs with source rocks deposited prior to 720 Ma. However, there is not an obvious physical explanation for why this would be a time dependent process. Further, disequilibrium melting processes have been documented and studied in exhumed Phanerozoic orogens (Ayres and Harris, 1997; Watson et al., 1989; Zeng et al., 2005).

4.2. Entrainment of residual apatite

Last, it is conceivable that residual apatite may become entrained in the escaping melt fraction, and the bulk P_2O_5 concentration of the magma will not be those of the liquids, rather a mixture of melt and restitic minerals (Chappell et al., 1987; Harrison and Watson, 1984; White and Chappell, 1977). Although entrainment of isolated apatite crystals is considered unlikely due to the high solubility of apatite in peraluminous melts (Pichavant et al., 1992; Wolf and London, 1994), apatite may be enclosed within other entrained restitic phases (Fig. 3b) and restitic phosphorus-bearing garnet or feldspar could also be entrained. Entrainment of these phases would increase the P_2O_5 of the bulk magma. On average, one would expect that a metasedimentary source with higher P_2O_5 concentrations and thus modal abundances of apatite (and/or phosphorus-bearing silicates), upon partial melting would produce granitic melts with a higher chance of incorporating phosphorus-rich restitic minerals. For the SPGs compilation presented here, restitic phosphate entrainment (if occurring) would have had a more pronounced effect on the P_2O_5 concentrations of Phanerozoic SPGs derived from post-720 Ma metasedimentary sources with higher phosphorus concentrations (*i.e.*, Group 3 and likely many Group 4 SPGs). In this scenario, although the higher P_2O_5 concentrations in the SPGs do not necessarily represent melt concentrations, but rather bulk magma concentrations, they would still reflect the higher amounts of phosphorus of their sources.

4.3. Phosphorus during crystallization-differentiation and cooling of granitic magmas

After an anatectic peraluminous granitic melt is extracted from its metasedimentary source region, its phosphorus concentrations can then be influenced through crystallization, differentiation, and cooling with the resulting effect that the final solidified granite may have a P_2O_5 concentration that is not that of the initial partial melt (Fig. 3c). The solidified granite will reflect a combination of (1) enrichment in melt P_2O_5 during differentiation, (2) near- to sub-solidus phosphorus loss via vapor exsolution, and (3) sub-solidus alteration. Below I consider how each of these processes could influence the interpretation of the SPG compilation.

First, the solubility of apatite in magmas has been known for decades to be influenced primarily by melt composition and temperature (Harrison and Watson, 1984; Pichavant et al., 1992; Watson, 1979; Wolf and London, 1994). The solubility of apatite decreases as melt SiO_2 increases (Harrison and Watson, 1984), but increases as melt ASI values increase (London, 1989; Pichavant et al., 1992; Wolf and London, 1994). In "I-type" or metaluminous systems, the P_2O_5 concentrations of basalts and andesites will increase until apatite saturation is reached (generally around 60-65 wt.% SiO_2). When the melt saturates in apatite, P_2O_5 concentrations begin to decrease and, if differentiation continues, results in silicic melts (>70 wt.% SiO_2) with <0.1 wt.% P_2O_5 (Bea et al., 1992; Lee and Bachmann, 2014). In contrast, in peraluminous melts the solubility of apatite is enhanced due to the formation of $AlPO_4$ complexes, so that a granitic melt with an ASI of 1.3 can have up to ~0.63 wt.% P_2O_5 at apatite saturation (following saturation models of Wolf and London, 1994). Pichavant et al. (1992) measured even higher melt P_2O_5 at apatite saturation of 0.9-1.2 wt.% at 780 °C in melts with an ASI of ~1.3. Indeed, it has been long established that despite their high silica content many Phanerozoic SPGs are notably enriched in phosphorus (Bea et al., 1992; London, 1992). As a striking example, quenched glasses from peraluminous obsidian glasses from the Macusani volcanic centre contain up to 0.58 wt.% P_2O_5 yet they do not contain apatite (London et al., 1988).

A pure partial melt of metasedimentary rocks will have high ASI values (e.g., ~1.1-1.4; (Acosta-Vigil et al., 2003; Patino-Douce and Harris, 1998) and its P_2O_5 concentrations may or may not be at apatite saturation depending on the P_2O_5 of the source (see discussion in section 4.1). Indeed, apatite is generally not a liquidus phase in many SPG plutons and only appears as a late-stage phase (though it may be abundant; Bea et al., 1994; London, 1992). During differentiation of a peraluminous granite melt, the ASI of the melt increases due to crystallization of assemblages with bulk ASI values of ~1 (e.g., quartz + feldspar + biotite), resulting in enhanced apatite solubility and increasing phosphorus concentrations (Bea et al., 1994). This is in accordance with the observation that within individual SPG plutons and associated pegmatites, P_2O_5 concentrations increase with increasing degree of fractionation (Bea et al., 1994). For example, phosphorus enrichment during

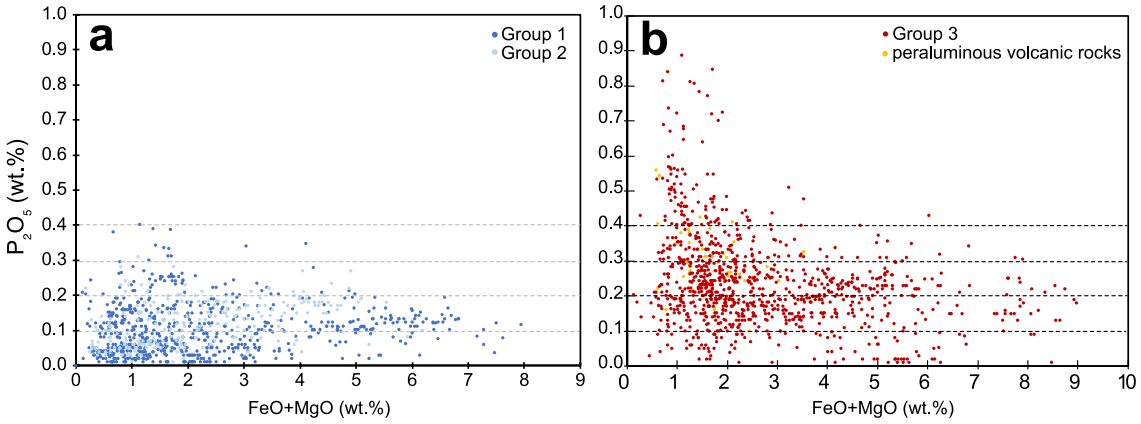

Fig. 5. P_2O_5 concentrations in SPGs and peraluminous volcanic rocks versus bulk-rock FeO+MgO. (a) Groups 1 and 2 and (b) Group 3 and peraluminous volcanic rocks. Grey horizontal dashed lines are for reference only.

crystallization-differentiation of strongly peraluminous granite plutons has been exhaustively demonstrated for the Pedrobernardo pluton (Bea et al., 1994) and Albuquerque batholith (London et al., 1999) in Spain.

Thus, in suites of strongly peraluminous granites, a primary magmatic process of concern for the interpretation of P_2O_5 concentrations is differentiation. In comparing SPGs from different groups, it is critical to assess whether the samples have experienced a similar degree of differentiation. During differentiation of peraluminous granitic melts, FeO, MgO, TiO_2, and CaO decrease and ASI increases (e.g., Bea et al., 1994; Champion and Bultitude, 2013) due to the differentiation of mafic silicates and Fe-Ti oxides, as well as, silicates with ASI values near 1 (e.g., feldspars). In terms of trace elements, incompatible elements such as Li, Rb, Cs, Tl, Sn, W, and Ga increase, whereas elements compatible in feldspars (Sr and Ba) decrease (Bea et al., 1994; Breaks and Moore, 1992; Champion and Bultitude, 2013).

To test whether different degrees of differentiation are causing the temporal trends observed in the SPG record (i.e., whether Group 3 is characterized by more differentiated granites), I consider bulk-rock P_2O_5 in the context of bulk-rock FeO+MgO, ASI, and K/Rb ratios. K/Rb values are widely used as an indicator of degree of granite differentiation due to the highly incompatible nature of Rb with values less than ~100 indicating extensive differentiation (Irber, 1999; Tartèse and Boulvais, 2010). Although, Nb/Ta and Zr/Hf ratios have been shown to decrease in strongly peraluminous granites during fractional crystallization due to the fractionation of biotite and/or muscovite and zircon (Ballouard et al., 2016; Tartèse and Boulvais, 2010), most samples in the compilation do not have data for these elements and thus these ratios are limited in their utility for assessing differentiation. Admittedly, this exercise assumes that the bulk-rock values are representative of melt compositions, which is certainly not true for all the compiled samples. However, these metrics in bulk-rock analyses have proved useful for tracking differentiation in previous studies of SPGs (Bea et al., 1994; Breaks and Moore, 1992; Champion and Bultitude, 2013).

First, experimental studies have demonstrated that partial melts of metasedimentary rocks at crustal pressures and temperatures are characterized by felsic compositions with low total FeO+MgO (<4 wt.%; see compilation of Gao et al., 2016). SPG bulk-rock values above this have been previously shown to be due to entrainment of restitic or peritectic phases such as garnet (Stevens et al., 2007). A minority of the samples in the compilation have FeO+MgO > 4 wt.% (20%; Fig. 5). These are not excluded, however, as their P_2O_5 concentrations are not distinctly different that those of SPGs with FeO+MgO < 4 wt.% (Fig. 5). P_2O_5 concentrations in Group 1 & 2 versus Group 3 are lower across a wide array of FeO+MgO. At FeO+MgO values less than ~1 to 1.5 wt.%, Group 3 SPG P_2O_5 concentrations increase (Fig. 5b). A similar increase is not observed in Group 1 and 2 SPGs (Fig. 5a). However, if only samples with FeO+MgO between 1 and 4 wt.% are considered, average P_2O_5 concentrations of samples from Group 1 & 2 (0.102±0.006 and 0.114±0.008, 2 s.e.m.) remain distinctly lower than those in Group 3 (0.262±0.012, 2 s.e.m.).

A similar exercise can be conducted with ASI values. Average ASI values across Groups 1, 2, and 3 are within error of each other (1.213±0.030, 1.189±0.030, 1.248±0.027, respectively). Further, localities with similar average ASI values show distinct difference in P_2O_5 concentrations between Groups 1 and 2 versus 3 (Fig. 6a). If analyses from different groups are binned by ASI values, Group 1 and 2 samples display lower average P_2O_5 concentrations compared to Group 3 across ASI values between 1.1 to 1.7 (Fig. 6b). This suggests that differences in ASI (as a potential proxy for both differentiation and enhanced apatite solubility) are not controlling the variations in P_2O_5 concentrations between Groups 1 and 2 versus 3.

Last, locality averages from Groups 1 and 2 on average have K/Rb ratios of 233±4 and 196±6 (2 s.e.m.), respectively, as compared to 161±20 (2. s.e.m.) for Group 3. If only samples with measured K/Rb ratios are considered, P_2O_5 concentrations increase dramatically at K/Rb ratios of <100 in Group 3 samples (Fig. 7b). Relatively few samples exist in Group 1 and 2 with measured K/Rb samples <100 (n = 72), but the limited number that do exist have similar P_2O_5 concentrations to those with K/Rb ratios >100 (Fig. 7b). At a given K/Rb ratio, average P_2O_5 concentrations of analyses binned by K/Rb ratios are lower in Groups 1 and 2 compared to Group 3 across a range all K/Rb ratios (Fig. 7b). This suggests that Group 3 SPG P_2O_5 concentrations are elevated compared to Groups 1 and 2 across a wide range of differentiation (and becomes more pronounced when strongly fractionated samples are considered). If strongly differentiated samples with K/Rb ratios <100 are removed from the compilation (leaving 1651 samples and 135 localities total in Groups 1, 2, and 3), the average bulk-rock P_2O_5 concentrations for locality averages in Groups 1, 2, and 3 are 0.095±0.011, 0.100±0.020, and 0.219±0.029, respectively (Fig. 7c) (see Table S2). These means are not distinguishable from the unfiltered dataset, suggesting that varying degrees of differentiation (as monitored by K/Rb ratios) are not controlling variations in bulk-rock P_2O_5 concentrations between different groups (Fig. 7b).

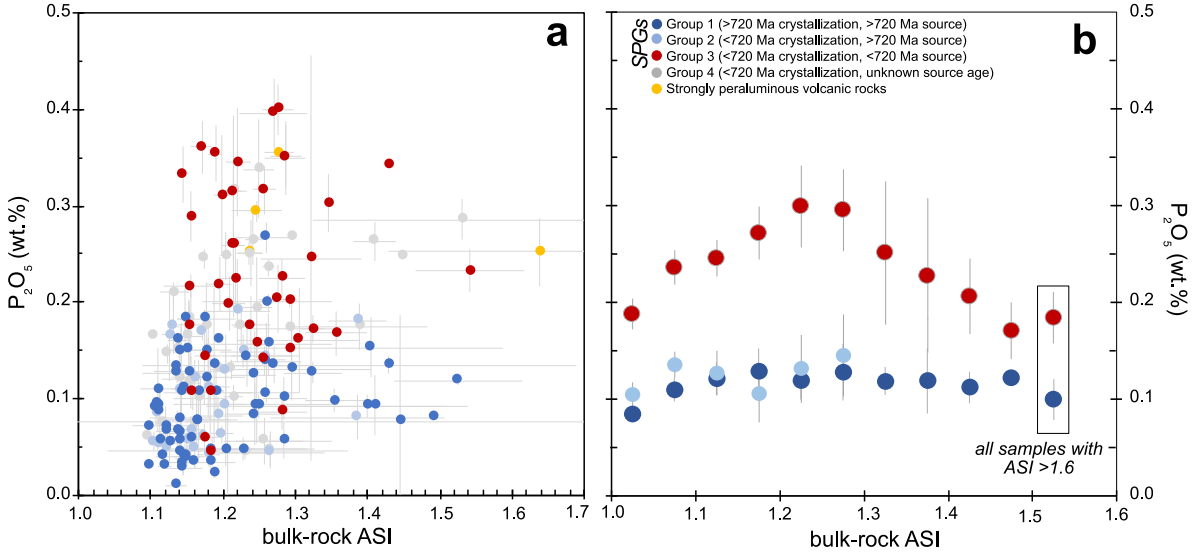

Fig. 6. P_2O_5 concentrations in SPGs and peraluminous volcanic rocks versus bulk-rock ASI values. (a) Average P_2O_5 concentrations versus ASI values for compiled localities. Error bars are 2 standard errors. Means and standard errors are given in Table S2. (b) Average P_2O_5 of all compiled analyses binned by bulk-rock ASI values. ASI bins are 0.05 increments and error bars are 2 standard errors. No averages are shown for Group 2 above ASI values of 1.3 due to the limited number of samples in that range (n = 10). Averages plotted above ASI values of 1.5 are for all samples with ASI values >1.5. These were binned together due to the limited number of samples with ASI values in that range (n = ~30 for Groups 1 and 3).

4.4. Near- to sub-solidus processes and preservation bias

Last, I briefly consider the effects of volatile exsolution and subsolidus alteration. First, insignificant portioning of phosphorus into a vapor during exsolution is expected as aqueous vapor-peraluminous melt partition coefficients for P (P_{vapor}/P_{melt}) are low (0.2-0.5 at 200 MPa; London et al., 1988). Second, although whole-rock P_2O_5 values during sericitic and argillic alteration of alkali-feldspars may decrease (London, 1992), there is no a priori reason to believe that this is occurring preferentially in Group 1 and 2 SPGs.

Finally, in this, and any other large compilation relying on the extant rock record, there is the possibility of preservation bias. However, there is not an obvious a priori reason why SPGs with lower P_2O_5 concentrations would be preferentially preserved prior to 720 Ma. Indeed, Cox et al. (2018) demonstrated that average P_2O_5 concentrations in all felsic igneous rocks have not varied significantly through time.

4.5. Summary

The magmatic and subsolidus processes described above may all play a role in modulating the final P_2O_5 concentrations of SPGs. However, there is only one process that is expected to be time variant and consistent with elevated phosphorus concentrations in Group 3 (and 4) SPGs: variations in metasedimentary source phosphorus abundances. Based on the discussion above, SPGs derived from post-720 Ma metasedimentary sources richer in phosphorus, should on average, have higher phosphorus concentrations either due to higher primary anatectic melt P_2O_5 concentrations (consistent with being saturated with apatite, see 4.1 and Fig. 4) and/or entrainment of restitic material richer in phosphorus. Thus, although there are certainly many caveats to interpreting SPG bulk-rock phosphorus concentrations, the difference in P_2O_5 of SPGs with pre- and post-720 Ma source rocks is most simply explained through differences in the primary phosphorus contents of their metasedimentary source rocks. This argument is strongly supported by the similarities in bulk-rock P_2O_5 of Group 1 & 2 SPGs (thought to be derived from pre-720 Ma sources despite their range in crystallization ages) as compared to Group 3 SPGs. The distribution of P_2O_5 in Group 4 SPGs are more similar to Group 3 SPGs, suggesting that many of these localities likely had sedimentary sources with young (<720 Ma) depositional ages. The fact that phosphorus concentrations in SPGs are to a first order controlled by phosphorus concentrations in their sedimentary source rocks is an important finding as this is not necessarily expected due to the multitude of fractionations that can happen from sedimentary source to final granite formation. This coevolution between sedimentary and SPG phosphorus records can now be used to inform both our understanding of the global phosphorus cycle and the interpretation of phosphorus concentrations in the igneous rock record.

5. Implications for the global phosphorus cycle

Source rocks for SPGs are typically shales or greywackes deposited in rift basins, basins marginal to magmatic arcs, or as turbidites adjacent to continental shelves. SPGs offer a complementary record to that of ancient sedimentary rocks in that they integrate large volumes of sedimentary successions that are distinct from marginal, potentially isolated, marine basins, typically preserved in the sedimentary record, which are likely not representative of bulk sedimentary trends. The compilation presented here supports previous observations of an increase in phosphorus concentrations in siliciclastic sedimentary rocks between 700-800 million years ago (Reinhard et al., 2017) and suggests that this increase was also characteristic of large volumes of continental shelf and slope sediments. Although the details behind the increase in phosphorus concentrations in sedimentary rocks are debated, proposed mechanisms link low phosphorus concentrations in pre-720 Ma siliciclastic rocks to low dissolved O_2 in seawater (Kipp and Stüeken, 2017; Reinhard et al., 2017). Interestingly, there is one locality in the Paleoproterozoic with anomalously high average P_2O_5 concentrations (>0.20 wt.%) for that time. This time also coincides with an increase in global phosphorite occurrences, potentially linked to a transient rise in dissolved O_2 and phosphorus levels, suggesting that the SPG record may have captured transiently high marine phosphorus concentrations (Holland, 2005).

SPGs also inform our understanding of how recycling of sedimentary rocks into the igneous crustal record may have var-

ied throughout Earth history. The findings here suggest that until the late Neoproterozoic, intracrustal recycling of sedimentary phosphorus was limited. Significant recycling of sedimentary material into igneous rocks occurred during the amalgamation of three supercontinents in the Precambrian (Kenorland at 2.7-2.5 Ga, Nuna/Columbia at 2.2-1.7 Ga, and Rodinia at 1.1-0.9 Ga) (Spencer et al., 2014), however enhanced recycling of sedimentary phosphorus into magmas only began with the construction of Gondwana and Pangea in the Neoproterozoic to Paleozoic. With the onset of phosphorus sequestration in marginal marine sediments in the Neoproterozoic, phosphorus could then be recycled to the continents during accretionary and collisional events. Some phosphorus could be stored in the crust in (meta-)sedimentary rocks, but also recycled into magmas through assimilation or partial melting. This recycled phosphorus would then be available for weathering (upon uplift and exposure) and kept in the surface environment to further fuel primary productivity. Thus, the enhanced sequestration of phosphorus into continental shelf and slope sediments beginning in the Neoproterozoic produced positive feedback whereby phosphorus could be more readily recycled to the continents for weathering and returned to the marine phosphorus reservoir.

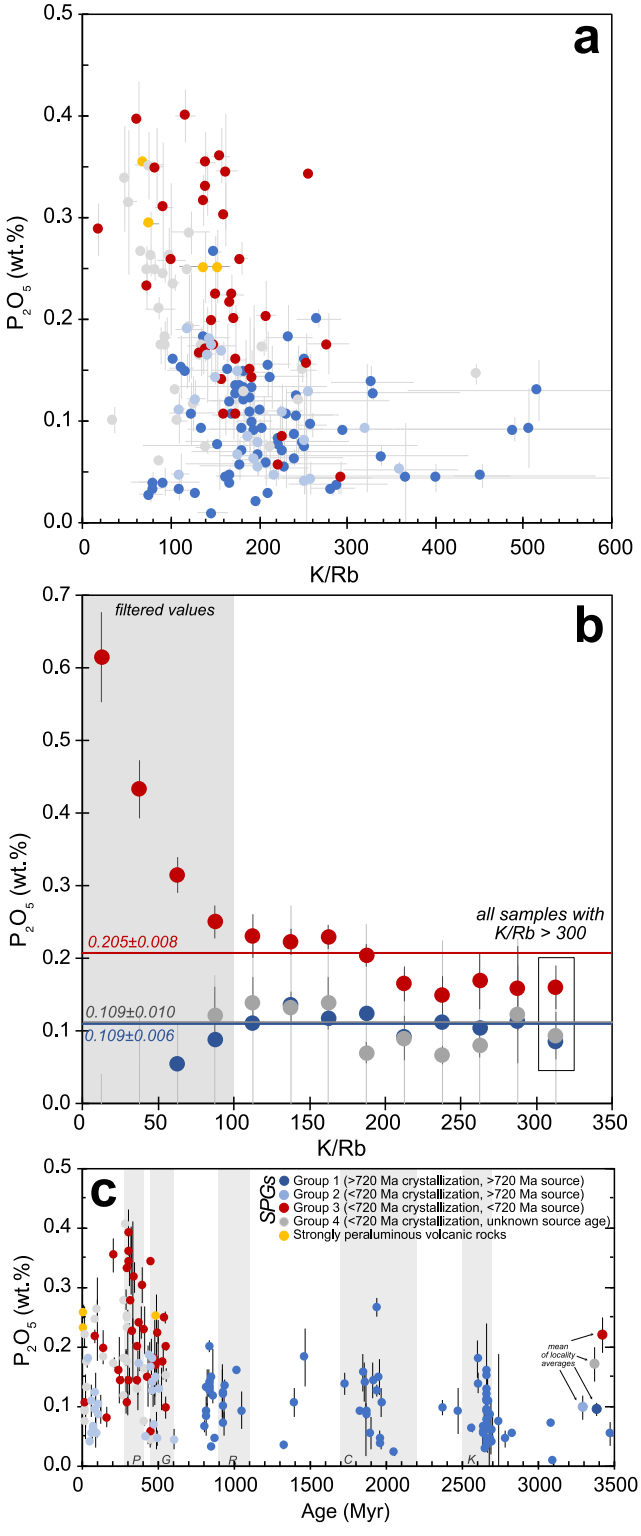

6. Implications for interpreting phosphorus in the igneous record

Moving beyond the sedimentary record, phosphorus concentrations in granites have been used to distinguish strongly peraluminous "S-type" from metaluminous "I-type granites" (Bea et al., 1992; Broska et al., 2004; London, 1992; Sha and Chappell, 1999). As discussed previously, phosphorus concentrates in peraluminous melts during differentiation due to the lack of apatite precipitation, a trend contrary to that observed in metaluminous melts. However, the results presented here suggest that pre-720 Ma SPGs (and SPGs with post-720 Ma crystallization ages but pre-720 Ma source rocks) do not typically have high P_2O_5 concentrations (on average ~0.10 wt.%), comparable to that of "I-type" granites (Lee and Bachman, 2014). Thus, phosphorus concentrations on their own are not particularly diagnostic of granite type.

Further, it has been recently proposed that phosphorus concentrations in zircon can be used as a diagnostic of criteria for derivation from peraluminous "S-type" versus metaluminous "I-type" melts (Burnham and Berry, 2017). Assuming equivalent zircon-melt phosphorus partition coefficients in metaluminous and peraluminous granitic magmas, zircon crystallizing in equilibrium from phosphorus-rich peraluminous granitic melts should also have higher phosphorus concentrations than those crystallizing from metaluminous granitic melts (Burnham and Berry, 2017). Indeed, phosphorus in zircon from peraluminous "S-type" versus metaluminous "I-type" granites from the Paleozoic Lachlan Fold Belt (Australia) (Burnham and Berry, 2017) and Lusatian granites (Germany) (Zhu et al., 2020) have higher phosphorus (mean concentrations of 1000±490 ppm versus 370±220 ppm). However, as demonstrated here, P_2O_5 concentrations in Group 1 and 2 SPGs are low and if it is assumed that this reflects to some degree lower melt phosphorus concentrations, then the phosphorus in zircon diagnostic criteria may not be useful to identify zircon derived from peraluminous melts derived from pre-720 Ma metasedimentary sources. This could require a critical reevaluation of studies where the use of zircon phosphorus concentrations to identify I-type (metaluminous) versus S-type (peraluminous) sources has been applied to

Fig. 7. K/Rb values as a monitor for differentiation (a) Locality average P_2O_5 concentrations in SPGs and peraluminous volcanic rocks versus bulk-rock K/Rb values. Locality averages are given in Table S2. Error bars are 2 standard errors. (b) Average P_2O_5 of all compiled analyses binned by bulk-rock K/Rb values. Samples are binned by K/Rb increments of 25 and error bars are 2 standard errors. No averages are shown for Group 1 & 2 below 50 and 75 respectively as only a few samples exist with K/Rb values in those ranges. Averages plotted at K/Rb values above 300 are for all samples with K/Rb values >300. These were binned together due to the limited number of samples with K/Rb values in that range. The grey shaded region indicates samples that were filtered from the compilation in panel c of this figure. Horizontal bars indicate mean P_2O_5 concentrations (±2 s.e.m.) for samples with K/Rb values >100 for Groups 1, 2, and 3. (c) Average P_2O_5 concentrations for SPG and peraluminous volcanic localities only including samples with K/Rb > 100 plotted against their crystallization ages. Error bars are 2 s.e.m. (see Table S2). Averages of Group 1, 2, 3, and 4 locality averages are shown on left side of the figure as large coloured circles. Error bars are 2 s.e.m. Compared to Fig. 1b, the temporal trend of increasing maximum P_2O_5 concentrations of locality averages remains, even after filtering. Grey bars as in Fig. 1b.

detrital zircon covering earlier periods in Earth history. For example, relatively low phosphorus concentrations in detrital zircon from the Hadean Jack Hills (Burnham and Berry, 2017) and Proterozoic and Archean (Zhu et al., 2020) have been used to infer that peraluminous granites were not abundant during these time periods. However, the low phosphorus concentrations in zircon from these time periods may simply be due to the lack of availability of sedimentary phosphorus to be transferred into peraluminous granitic melt. As SPGs predominantly form during collisional orogenesis or continental arc magmatism, an accurate understanding of their temporal distribution is important in understanding the evolution of tectonic regimes on Earth and crustal recycling through time (Bucholz and Spencer, 2019; Frost and Da Prat, 2021).

7. Conclusions

The presented compilation of phosphorus concentrations in strongly peraluminous granites (SPGs) from the past ~3.5 billion years demonstrate an abrupt increase in maximum phosphorus concentrations after 720 Ma. Analysis of metamorphic, magmatic, and subsolidus processes on the bulk-rock P_2O_5 concentrations of SPGs suggest that the lower average bulk-rock P_2O_5 concentrations SPGs sources derived from metasedimentary rocks deposited prior to ~720 Ma likely reflects lower phosphorus concentrations of their metasedimentary sources. This SPG compilation is consistent with previous observations of phosphorus abundances in the marine sedimentary record, provides an alternative archive in that SPGs form through the partial melting of (relatively) large volumes of continental shelf to slope sedimentary rocks, and represents an example of how temporal changes in biogeochemical cycles on the Earth's surface can be imprinted on an important class of igneous rocks. The SPG compilation also documents a clear shift in the crustal phosphorus cycle with the onset of enhanced recycling of sedimentary phosphorus into the igneous crust in the Neoproterozoic to Phanerozoic, where it can be again weathered and returned to the ocean to fuel further photosynthesis. The compilation also indicates that despite previous suggestion that phosphorus concentrations can be used to distinguish between strongly peraluminous "S-type" versus metaluminous "I-type" granites (as well as zircon that crystallizes in from magmas of these compositions), phosphorus concentrations on their own are not diagnostic of granite sources. Future work analyzing phosphorus in zircon from Archean and Proterozoic SPGs is required to test this hypothesis.

CRediT authorship contribution statement

Claire E. Bucholz: Conceptualization, Formal analysis, Funding acquisition, Methodology, Writing – original draft.

Declaration of competing interest

The authors declare that they have no known competing financial interests or personal relationships that could have appeared to influence the work reported in this paper.

Data availability

Data used is provided as a supplementary file.

Acknowledgements

The author thanks Rahul Chawlani for assistance with the XRF analyses and Chris Yakymchuk for discussions and contribution of new modelling results included in this paper. The author is grateful to Woody Fischer and Michael Kipp for discussions on the sedimentary phosphorus cycle. The author also thanks Omar Bartoli and Antonio Acosta-Vigil for thoughtful and constructive reviews of the manuscript, as well as, Michel Pichavant for a critical review of a previous version of this manuscript that helped greatly to clarify and strengthen the arguments within. Funding: This work was supported by NSF grant EAR-1943629.

Appendix A. Supplementary material

Supplementary material related to this article can be found online at https://doi.org/10.1016/j.epsl.2022.117795.

References

Acosta-Vigil, A., Buick, I., Hermann, J., Cesare, B., Rubatto, D., London, D., Morgan, G.B., 2010. Mechanisms of crustal anatexis: a geochemical study of partially melted metapelitic enclaves and host dacite, SE Spain. J. Petrol. 51, 785–821. https://doi.org/10.1093/petrology/egp095.

Acosta-Vigil, A., Cesare, B., London, D., Morgan, G.B., 2007. Microstructures and composition of melt inclusions in a crustal anatectic environment, represented by metapelitic enclaves within El Hoyazo dacites, SE Spain. Chem. Geol. 237, 450–465. https://doi.org/10.1016/j.chemgeo.2006.07.014.

Acosta-Vigil, A., London, D., Morgan, G.B., Dewers, T.A., 2003. Solubility of excess alumina in hydrous granitic melts in equilibrium with peraluminous minerals at 700–800 °C and 200 MPa, and applications of the aluminum saturation index. Contrib. Mineral. Petrol. 146, 100–119. https://doi.org/10.1007/s00410-003-0486-6.

Ague, J.J., 2017. Element mobility during regional metamorphism in crustal and subduction zone environments with a focus on the rare earth elements (REE). Am. Mineral. 102 (9), 1796–1821.

Ayres, M., Harris, N., 1997. REE fractionation and Nd-isotope disequilibrium during crustal anatexis: constraints from Himalayan leucogranites. Chem. Geol. 139, 249–269. https://doi.org/10.1016/S0009-2541(97)00038-7.

Ballouard, C., Poujol, M., Boulvais, P., Branquet, Y., Tartèse, R., Vigneresse, J.-L., 2016. Nb-Ta fractionation in peraluminous granites: a marker of the magmatic-hydrothermal transition. Geology 44, 231–234. https://doi.org/10.1130/G37475.1.

Bartoli, O., 2021. Granite geochemistry is not diagnostic of the role of water in the source. Earth Planet. Sci. Lett. 564, 116927. https://doi.org/10.1016/j.epsl.2021.116927.

Bartoli, O., Cesare, B., Poli, S., Bodnar, R.J., Acosta-Vigil, A., Frezzotti, M.L., Meli, S., 2013. Recovering the composition of melt and the fluid regime at the onset of crustal anatexis and S-type granite formation. Geology 41, 115–118. https://doi.org/10.1130/G33455.1.

Bea, F., 1996. Residence of REE, Y, Th and U in granites and crustal protoliths; implications for the chemistry of crustal melts. J. Petrol. 57, 521–552.

Bea, F., Fershtater, G., Corretgé, L.G., 1992. The geochemistry of phosphorus in granite rocks and the effect of aluminium. Lithos 29, 43–56. https://doi.org/10.1016/0024-4937(92)90033-U.

Bea, F., Montero, P., 1999. Behavior of accessory phases and redistribution of Zr, REE, Y, Th, and U during metamorphism and partial melting of metapelites in the lower crust: an example from the Kinzigite formation of Ivrea-Verbano, NW Italy. Geochim. Cosmochim. Acta 63, 1133–1153. https://doi.org/10.1016/S0016-7037(98)00292-0.

Bea, F., Pereira, M.D., Corretgé, L.G., Fershtater, G.B., 1994. Differentiation of strongly peraluminous, perphosphorus granites: the pedrobernardo pluton, central Spain. Geochim. Cosmochim. Acta 58, 2609–2627. https://doi.org/10.1016/0016-7037(94)90132-5.

Bjerrum, C.J., Canfield, D.E., 2002. Ocean productivity before about 1.9 Gyr ago limited by phosphorus adsorption onto iron oxides. Nature 417, 159–162. https://doi.org/10.1038/417159a.

Breaks, F.W., Moore, J.M., 1992. The ghost lake batholith, superior province of northwestern Ontario: a fertile, S-type, peraluminous granite - rare-element pegmatite system. Can. Mineral. 30, 835–875.

Broska, I., Williams, C.T., Uher, P., Konečný, P., Leichmann, J., 2004. The geochemistry of phosphorus in different granite suites of the Western Carpathians, Slovakia: the role of apatite and P-bearing feldspar. Chem. Geol. 205, 1–15. https://doi.org/10.1016/j.chemgeo.2003.09.004.

Bucholz, C.E., Spencer, C.J., 2019. Strongly peraluminous granites across the Prchean–Proterozoic transition. J. Petrol. 60, 1299–1348. https://doi.org/10.1093/petrology/egz033.

Burnham, A.D., Berry, A.J., 2017. Formation of Hadean granites by melting of igneous crust. Nat. Geosci. 10, 457–461. https://doi.org/10.1038/ngeo2942.

Cesare, B., Acosta-Vigil, A., Bartoli, O., Ferrero, S., 2015. What can we learn from melt inclusions in migmatites and granulites? Lithos 239, 186–216. https://doi.org/10.1016/j.lithos.2015.09.028.

Champion, D.C., Bultitude, R.J., 2013. The geochemical and SrNd isotopic characteristics of Paleozoic fractionated S-types granites of North Queensland: implications for S-type granite petrogenesis. Lithos 162–163, 37–56. https://doi.org/10.1016/j.lithos.2012.11.022.

Chappell, B.W., White, A.J.R., 1992. I- and S-type granites in the Lachlan Fold Belt. Trans. R. Soc. Edinb. Earth Sci. 83, 1–26. https://doi.org/10.1016/0016-7037(82)90301-5.

Chappell, B.W., White, A.J.R., Wyborn, D., 1987. The importance of residual source material (restite) in granite petrogenesis. J. Petrol. 28, 1111–1138. https://doi.org/10.1093/petrology/28.6.1111.

Cook, P.J., McElhinny, M.W., 1979. A reevaluation of the spatial and temporal distribution of sedimentary phosphate deposits in the light of plate tectonics. Econ. Geol. 74, 315–330. https://doi.org/10.2113/gsecongeo.74.2.315.

Cox, G.M., Lyons, T.W., Mitchell, R.N., Hasterok, D., Gard, M., 2018. Linking the rise of atmospheric oxygen to growth in the continental phosphorus inventory. Earth Planet. Sci. Lett. 489, 28–36. https://doi.org/10.1016/j.epsl.2018.02.016.

Duc-Tin, Q., Keppler, H., 2015. Monazite and xenotime solubility in granitic melts and the origin of the lanthanide tetrad effect. Contrib. Mineral. Petrol. 169, 8. https://doi.org/10.1007/s00410-014-1100-9.

Frost, B.R., Barnes, C.G., Collins, W.J., Arculus, R.J., Ellis, D.J., Frost, C.D., 2001. A geochemical classification for granitic rocks. J. Petrol. 42, 2033–2048. https://doi.org/10.1093/petrology/42.11.2033.

Frost, C.D., Da Prat, F.A., 2021. Petrogenetic and tectonic interpretation of strongly peraluminous granitic rocks and their significance in the Archean rock record. Am. Mineral. 106, 1195–1208. https://doi.org/10.2138/am-2022-8001.

Gao, P., Zheng, Y., Zhao, Z., 2016. Experimental melts from crustal rocks: a lithochemical constraint on granite petrogenesis. Lithos 266–267, 133–157. https://doi.org/10.1016/j.lithos.2016.10.005.

Gianola, O., Bartoli, O., Ferri, F., Galli, A., Ferrero, S., Capizzi, L.S., Liebske, C., Remusat, L., Poli, S., Cesare, B., 2021. Anatectic melt inclusions in ultra high temperature granulites. J. Metamorph. Geol. 39, 321–342. https://doi.org/10.1111/jmg.12567.

Halevy, I., Alesker, M., Schuster, E.M., Popovitz-Biro, R., Feldman, Y., 2017. A key role for green rust in the Precambrian oceans and the genesis of iron formations. Nat. Geosci. 10, 135–139. https://doi.org/10.1038/ngeo2878.

Harrison, M.T., Watson, B.E., 1984. The behavior of apatite during crustal anatexis: equilibrium and kinetic considerations. Geochim. Cosmochim. Acta 48, 1467–1477. https://doi.org/10.1016/0016-7037(84)90403-4.

Holland, H.D., 2005. 100th anniversary special paper: sedimentary mineral deposits and the evolution of Earth's near surface environments. Econ. Geol. 100, 1489–1509.

Hopkinson, T.N., Harris, N.B.W., Warren, C.J., Spencer, C.J., Roberts, N.M.W., Horstwood, M.S.A., Parrish, R.R., Eimf, 2017. The identification and significance of pure sediment-derived granites. Earth Planet. Sci. Lett. 467, 57–63. https://doi.org/10.1016/j.epsl.2017.03.018.

Horton, F., 2015. Did phosphorus derived from the weathering of large igneous provinces fertilize the Neoproterozoic ocean? Geochem. Geophys. Geosyst. 16, 1723–1738. https://doi.org/10.1002/2015GC005792.

Irber, W., 1999. The lanthanide tetrad effect and its correlation with K/Rb, Eu/Eu*, Sr/Eu, Y/Ho, and Zr/Hf of evolving peraluminous granite suites. Geochim. Cosmochim. Acta 63, 489–508. https://doi.org/10.1016/S0016-7037(99)00027-7.

Kipp, M.A., Stüeken, E.E., 2017. Biomass recycling and Earth's early phosphorus cycle. Sci. Adv. 3, eaao4795. https://doi.org/10.1126/sciadv.aao4795.

Kohn, M.J., Malloy, M.A., 2004. Formation of monazite via prograde metamorphic reactions among common silicates: implications for age determinations. Geochim. Cosmochim. Acta 68, 101–113. https://doi.org/10.1016/S0016-7037(03)00258-8.

Lee, C.-T.A., Bachmann, O., 2014. How important is the role of crystal fractionation in making intermediate magmas? Insights from Zr and P systematics. Earth Planet. Sci. Lett. 393, 266–274. https://doi.org/10.1016/j.epsl.2014.02.044.

London, D., 1992. Phosphorus in S-type magmas: the P2O5 content of feldspars from peraluminous magmas, pegmatite, and rhyolites. Am. Mineral. 77, 126–145.

London, D., 1989. Vapor-undersaturated experiments with Macusani glass + H20 at 200 MPa, and the internal differentiation of granitic pegmatites. Contrib. Mineral. Petrol. 102, 1–17.

London, D., Hervig, R.L., Morgan, G.B., 1988. Melt-vapor solubilities and elemental partitioning in peraluminous granite-pegmatite systems: experimental results with Macusani glass at 200 MPa. Contrib. Mineral. Petrol. 99, 360–373. https://doi.org/10.1007/BF00375368.

London, D., Wolf, M.B., Vi, G.B.M., Garrido, M.G., 1999. Experimental silicate–phosphate equilibria in peraluminous granitic magmas, with a case study of the Alburquerque Batholith at Tres Arroyos Badajoz, Spain 40, 26.

Montel, J.-M., 1993. A model for monazite/melt equilibrium and application to the generation of granitic magmas. Chem. Geol. 110, 127–146. https://doi.org/10.1016/0009-2541(93)90250-M.

Nabelek, Peter.I., Glascock, Michael.D., 1995. REE-depleted leucogranites, black hills, South Dakota: a consequence of disequilibrium melting of monazite-bearing schists. J. Petrol. 36, 1055–1071. https://doi.org/10.1093/petrology/36.4.1055.

Patino-Douce, A.E., Harris, N., 1998. Experimental constraints on Himalayan anatexis 39, 689–710.

Piccoli, P.M., Candela, P.A., 2002. Apatite in igneous systems. Rev. Mineral. Geochem. 48, 255–292. https://doi.org/10.2138/rmg.2002.48.6.

Pichavant, M., Kontak, Daniel J., Briqueu, Louis, Valencia, Jacinto, Clark, Alan H., 1988. The Miocene-Pliocene Macusani volcanics, SE Peru: II. Geochemistry and origing of a felsic peraluminous magma. Contrib. Mineral. Petrol. 100, 325–338.

Pichavant, M., Montel, J.-M., Richard, L.R., 1992. Apatite solubility in peraluminous liquids: experimental data and an extension of the Harrison-Watson model. Geochim. Cosmochim. Acta 56, 3855–3861. https://doi.org/10.1016/0016-7037(92)90178-L.

Planavsky, N.J., Rouxel, O.J., Bekker, A., Lalonde, S.V., Konhauser, K.O., Reinhard, C.T., Lyons, T.W., 2010. The evolution of the marine phosphate reservoir. Nature 467, 1088–1090. https://doi.org/10.1038/nature09485.

Pyle, J.M., Spear, F.S., 1999. Yttrium zoning in garnet: coupling of major and accessory phases during metamorphic reactions 49.

Rasmussen, B., Muhling, J.R., Suvorova, A., Fischer, W.W., 2021. Apatite nanoparticles in 3.46–2.46 Ga iron formations: evidence for phosphorus-rich hydrothermal plumes on early Earth. Geology 49, 647–651. https://doi.org/10.1130/G48374.1.

Reinhard, C.T., Planavsky, N.J., Gill, B.C., Ozaki, K., Robbins, L.J., Lyons, T.W., Fischer, W.W., Wang, C., Cole, D.B., Konhauser, K.O., 2017. Evolution of the global phosphorus cycle. Nature 541, 386–389. https://doi.org/10.1038/nature20772.

Sha, L.-K., Chappell, B.W., 1999. Apatite chemical composition, determined by electron microprobe and laser-ablation inductively coupled plasma mass spectrometry, as a probe into granite petrogenesis. Geochim. Cosmochim. Acta 63, 3861–3881. https://doi.org/10.1016/S0016-7037(99)00210-0.

Solar, G.S., Brown, M., 2001. Petrogenesis of migmatites in Maine, USA: possible source of peraluminous leucogranite in plutons? J. Petrol. 42 (4), 789–823.

Spear, F.S., Pyle, J.M., 2002. Apatite, monazite, and xenotime in metamorphic rocks. Rev. Mineral. Geochem. 48, 293–335. https://doi.org/10.2138/rmg.2002.48.7.

Spencer, C.J., Cawood, P.A., Hawkesworth, C.J., Raub, T.D., Prave, A.R., Roberts, N.M.W., 2014. Proterozoic onset of crustal reworking and collisional tectonics: reappraisal of the zircon oxygen isotope record. Geology 42, 451–454. https://doi.org/10.1130/G35363.1.

Stepanov, A.S., Hermann, J., Rubatto, D., Rapp, R.P., 2012. Experimental study of monazite/melt partitioning with implications for the REE, Th and U geochemistry of crustal rocks. Chem. Geol. 300–301, 200–220. https://doi.org/10.1016/j.chemgeo.2012.01.007.

Stevens, G., Villaros, A., Moyen, J.-F., 2007. Selective peritectic garnet entrainment as the origin of geochemical diversity in S-type granites. Geology 35, 9. https://doi.org/10.1130/G22959A.1.

Sylvester, P.J., 1998. Post-collisional strongly peraluminous granites. Lithos 45, 29–44. https://doi.org/10.1016/S0024-4937(98)00024-3.

Tartèse, R., Boulvais, P., 2010. Differentiation of peraluminous leucogranites "en route" to the surface. Lithos 114, 353–368. https://doi.org/10.1016/j.lithos.2009.09.011.

Tyrrell, T., 1999. The relative influences of nitrogen and phosphorus on oceanic primary production. Nature 400, 525–531.

Watson, E.B., 1979. Apatite saturation in basic to intermediate magmas. Geophys. Res. Lett. 6, 937–940. https://doi.org/10.1029/GL006i012p00937.

Watson, E.B., Capobianco, C.J., 1981. Phosphorus and the rare Earth elements in felsic magmas: an assessment of the role of apatite. Geochim. Cosmochim. Acta 45, 2349–2358. https://doi.org/10.1016/0016-7037(81)90088-0.

Watson, E.B., Vicenzi, E.P., Rapp, R.P., 1989. Inclusion/host relations involving accessory minerals in high-grade metamorphic and anatectic rocks. Contrib. Mineral. Petrol. 101, 220–231. https://doi.org/10.1007/BF00375308.

White, J.R., Chappell, B.W., 1977. Ultrametamorphism and granitoid genesis. Tectonophysics 43, 7–22.

Wing, B.A., Ferry, J.M., Harrison, T.M., 2003. Prograde destruction and formation of monazite and allanite during contact and regional metamorphism of pelites: petrology and geochronology. Contrib. Mineral. Petrol. 145, 228–250. https://doi.org/10.1007/s00410-003-0446-1.

Wolf, M.B., London, D., 1994. Apatite dissolution into peraluminous haplogranitic melts: an experimental study of solubilities and mechanisms. Geochim. Cosmochim. Acta 58, 4127–4145.

Yakymchuk, C., 2017. Behaviour of apatite during partial melting of metapelites and consequences for prograde suprasolidus monazite growth. Lithos 274–275, 412–426. https://doi.org/10.1016/j.lithos.2017.01.009.

Yakymchuk, C., Acosta-Vigil, A., 2019. Geochemistry of phosphorus and the behavior of apatite during crustal anatexis: insights from melt inclusions and nanogranitoids. Am. Mineral. 104, 1765–1780. https://doi.org/10.2138/am-2019-7054.

Zegeye, A., Bonneville, S., Benning, L.G., Sturm, A., Fowle, D.A., Jones, C., Canfield, D.E., Ruby, C., MacLean, L.C., Nomosatryo, S., Crowe, S.A., Poulton, S.W., 2012. Green rust formation controls nutrient availability in a ferruginous water column. Geology 40, 599–602. https://doi.org/10.1130/G32959.1.

Zeng, L., Saleeby, J.B., Asimow, P., 2005. Nd isotope disequilibrium during crustal anatexis: a record from the Goat Ranch migmatite complex, southern Sierra Nevada batholith, California. Geology 33, 53. https://doi.org/10.1130/G20831.1.

Zhang, C., Liu, D., Zhang, X., Spencer, C., Tang, M., Zeng, J., Jiang, S., Jolivet, M., Kong, X., 2020. Hafnium isotopic disequilibrium during sediment melting and assimilations. Geochem. Perspect. Lett., 34–39. https://doi.org/10.7185/geochemlet.2001.

Zhu, Z., Campbell, I.H., Allen, C.M., Burnham, A.D., 2020. S-type granites: their origin and distribution through time as determined from detrital zircons. Earth Planet. Sci. Lett. 536, 116140. https://doi.org/10.1016/j.epsl.2020.116140.